Impact of energy limitations on function and resilience in long-wavelength Photosystem II

Stefania Viola[a*], *William Roseby*[a], *Stefano Santabarabara*[b], *Dennis Nürnberg*[c], *Ricardo Assunção*[c], *Holger Dau*[c], *Julien Sellés*[d], *Alain Boussac*[e], *Andrea Fantuzzi*[a], *A William Rutherford*[a*]

[a]Department of Life Sciences, Imperial College, SW7 2AZ London, UK

[b]Istituto di Biofisica, Consiglio Nazionale delle Ricerche, 20133 Milano, Italy

[c]Physics Department, Freie Universität Berlin, 14195 Berlin, Germany

[d]Institut de Biologie Physico-Chimique, UMR CNRS 7141 and Sorbonne Université, 75005 Paris, France

[e]Institut de Biologie Intégrative de la Cellule, UMR9198, CEA Saclay, 91191 Gif-Sur-Yvette, France

[*]Corresponding Authors:

A.W. Rutherford, Department of Life Sciences, Imperial College London, London SW7 2AZ, UK, Tel +44 2075945329

E-mail:a.rutherford@imperial.ac.uk

S. Viola, Department of Life Sciences, Imperial College London, London SW7 2AZ, UK, Tel +44 2075941778

E-mail: s.viola@imperial.ac.uk

Keywords: Photosystem II, electron transfer, chlorophyll, cyanobacteria

Abstract

Photosystem II (PSII) uses the energy from red light (~680 nm) to split water and reduce quinone, an energy-demanding process based on chlorophyll a (Chl-a) photochemistry. Two kinds of cyanobacterial PSII can use Chl-d and Chl-f to perform the same reactions using lower energy, far-red light (~720 nm). PSII from *Acaryochloris marina* has Chl-d replacing all but one of its 35 Chl-a, while PSII from *Chrooccidiopsis thermalis*, a facultative far-red species, has just 4 Chl-f and 1 Chl-d replacing 5 of the 35 Chl-a. From bioenergetic considerations, the long-wavelength forms of PSII were predicted to lose photochemical efficiency and/or resilience to harmful light-induced charge recombination. Here, we compare enzyme turnover efficiency, forward electron transfer, back-reactions and photodamage in Chl-f-PSII, Chl-d-PSII and Chl-a-PSII. We show: i) all types of PSII have comparably efficient enzyme turnover; ii) the modified energy gaps on the acceptor side of Chl-d-PSII favor recombination by $P^{+}Phe^{-}$ repopulation and lead to increased singlet oxygen production and sensitivity to high light damage compared to Chl-a-PSII and Chl-f-PSII; ii) the acceptor side energy gaps in Chl-f-PSII are tuned to avoid harmful back reactions, favoring resilience to light damage over light usage efficiency. The results are explained by the differences in the redox tuning of the electron transfer cofactors Phe and Q_A and in the number and layout of the chlorophylls that share the excitation energy with the primary electron donor. PSII has adapted to low energy in two ways, each appropriate for its specific environment but with different functional penalties.

Significance statement

Photosystem II (PSII) is the enzyme that powers the planet. It uses chlorophyll to collect light and use its energy to do photochemistry. PSII extracts electrons from water, producing the oxygen that energizes the atmosphere, and feeds them into the process that fixes carbon dioxide into carbon polymers that are the fuels and building blocks of life. Virtually all PSIIs do photochemistry using red light, but two rare forms use lower energy, far-red light. The current study focuses on the efficiency and resilience of the low energy types of PSII compared to standard PSII. The findings are relevant to proposals to extend the spectrum of photosynthesis in crop plants and in potentially biotechnologically relevant cyanobacteria and algae.

1 – Introduction

Photosystem II (PSII) is the water/plastoquinone photo-oxidoreductase, the key energy converting enzyme in oxygenic photosynthesis. Standard PSII contains 35 chlorophylls a (Chl-a) and 2 pheophytins (Phe). Four of the Chl molecules (P_{D1}, P_{D2}, Chl_{D1} and Chl_{D2}) and both Phe molecules are located in the center of PSII (1). The remaining 31 Chl-a in the PSII core constitute a peripheral light-collecting antenna. When antenna chlorophylls are excited by absorbing a photon, they transfer the excitation energy to the primary electron donor chlorophyll (referred to as P), which appears to be Chl_{D1}, the red-most pigment in the reaction center, although it's been reported that charge separation from P_{D1} can occur in a fraction of centers (1–4). The charge separation is then progressively stabilized via a series of electron transfer steps (Fig. 1A) that lead to the reduction of plastoquinone and the oxidation of water.

PSII activity is energy demanding. Most of the energy gained from light absorption is required for the redox chemistry and the associated generation of proton motive force (~1eV), while the rest is released as heat to ensure the high quantum yield of the forward reactions and to avoid wasteful and damaging side- and back-reactions (5). Compared to other photosynthetic reaction centers, PSII seems to be energy deficient, hence its susceptibility to photodamage and its complex regulatory and protective mechanisms (5).

In Chl-a-PSII, the primary donor absorbs red photons at 680 nm, and this defines the energy available for photochemistry (1.82 eV). This was thought to be the minimum amount of energy required for an optimum balance of efficiency versus resilience to photodamage (5), explaining the "red limit" for oxygenic photosynthesis (5, 6).

The first reported case in which the red limit is exceeded was the Chl-d-containing cyanobacterium *Acaryochloris marina* (*A. marina*) (7). Chl-d-PSII contains 34 Chl-d and 1 Chl-a (proposed to be in the P_{D1} position (8)) and uses less energy, with the proposed Chl-d primary donor in the Chl_{D1} position absorbing far-red photons at ~720 nm (9), corresponding to an energy of ~1.72 eV (Fig. 1B).

Recently, it was discovered that certain cyanobacteria use an even more red-shifted pigment, Chl-f, in combination with Chl-a (10, 11). When grown in far-red light, these cyanobacteria replace their standard Chl-a containing PSII with Chl-f-PSII, that has far-red specific variants of the core protein subunits (D1, D2, CP43, CP47 and PsbH) and contains ~90% of Chl-a and ~10% of Chl-f (6, 11). The Chl-f-PSII from *Chroococcidiopsis thermalis* PCC7203 (*C. thermalis*), which contains 30 Chl-a, 4 Chl-f and 1 Chl-d, was shown to have a long wavelength primary donor (either Chl-f or d, in Chl_{D1} position) absorbing far-red photons at ~720 nm (Fig. 1C), the same wavelength as in *A. marina* (6, 12). A recent cryo-EM structure has also argued for Chl_{D1} being the single Chl-d in the far-red PSII of *Synechococcus elongatus* PCC7335 (13). The facultative, long-wavelength species that use Chl-f are thus the second case of oxygenic photosynthesis functioning beyond the red-limit (6), but the layout of their long wavelength pigments is quite different from the one of the Chl-d-PSII.

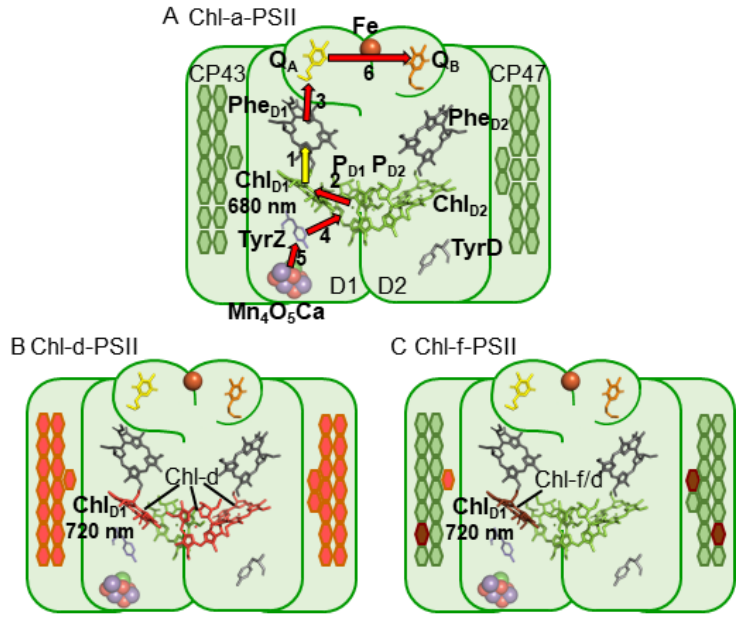

Fig. 1. The three types of PSII. (A) Chl-a-PSII (PDB ID: 3ARC, (14)) with the key cofactors of the reaction center, located in the subunits D1 and D2, labelled. Besides the P_{D1}, P_{D2}, Chl_{D1} and Chl_{D2} chlorophylls and the two pheophytins, Phe_{D1} and Phe_{D2}, these cofactors include the quinones, Q_A and Q_B, and the non-heme iron (Fe) on the acceptor side and the two redox-active tyrosines TyrZ and TyrD and the manganese cluster (Mn_4O_5Ca) on the donor side. The arrows represent the electron transfer steps and the numbers the order of the steps. The yellow arrow is the primary charge separation, with other steps shown as red arrows. The primary donor is shown as Chl_{D1}. (B) and (C) Chl-d-PSII and Chl-f-PSII, with the far-red chlorophylls in the reaction centers highlighted and the wavelength of the primary donor, assumed to be Chl_{D1}, indicated. The hexagons on the sides of each reaction center represent the chlorophylls of the respective antennas, located in the subunits CP43 and CP47. Chl-a is represented in green, Chl-d in orange and Chl-f in brown. In (C) the single Chl-d is located in the antenna, but the possibility that it is located in the Chl_{D1} position and plays the primary donor role also exists (6, 13) and the locations of the 4 antenna in the peripheral antenna are uncertain but reflect suggestions in the literature (6).

Assuming Chl-a-PSII already functions at an energy red limit (5), the diminished energy in Chl-d-PSII and Chl-f-PSII seems likely to exacerbate the energetic constraints. Thus, it was suggested that far-red PSII should have decreased photochemical efficiency and/or loss of resilience to photodamage (6, 15, 16). These energetic constraints need to be taken into account when considering engineering of far-red photosynthesis into other organisms of agricultural or technological interest (17).

Here we report a comparison of the enzyme turnover efficiency, forward reactions, and back-reactions in the three known types of PSII: the "standard" Chl-a-PSII, and the two far-red types, the Chl-f-PSII from *C. thermalis* and the Chl-d-PSII from *A. marina*.

2 - Results

2.1 - Fluorescence decay kinetics in the three types of PSII

Flash-induced fluorescence decay kinetics were compared in membranes from *A. marina*, white-light (WL) grown *C. thermalis* and far-red-light (FR) grown *C. thermalis*. When forward electron transfer occurs (Fig. 2A), the fluorescence decay comprises three phases (18, 19): the fast phase (~0.5 ms) is attributed to electron transfer from Q_A^- to Q_B or Q_B^- and the middle phase (~3 ms) is generally attributed to Q_A^- oxidation limited by plastoquinone (PQ) entry to an initially empty Q_B site and/or by Q_BH_2 exiting the site prior to PQ entry (20). These two phases had comparable time-constants in all samples (T1 = 0.5-0.6 and T2 = 3.5-5 ms, Table S1), with the middle phase being just slightly slower in *A. marina* and FR *C. thermalis*. This minor effect could reflect differences in the redox state of the PQ pool.

In *A. marina* membranes, the cumulative amplitude of these two phases was smaller because of the presence of a non-decaying component of the fluorescence, that did not return to the original F_0 level even at 100 s after the flash (Fig. S1). This non-decaying component, absent in the two *C. thermalis* samples, is attributed to centers without a functional Mn-cluster, in which P^+ is reduced by an electron donor that does not recombine in the minutes timescale (such as Mn^{2+}, TyrD, or the ChlZ/Car side-path), with the consequent stabilization of Q_A^- (21, 22).

The third decay phase is attributed to slow Q_A^- reoxidation due to charge recombination with the S_2 state of the Mn cluster in centers where forward electron transfer to Q_B/Q_B^- does not occur. This phase was slower in FR *C. thermalis* (T3 = 14.3±4.6 s) than in WL *C. thermalis* (T3 = 5.6±2.4 s) but had a similar amplitude in the two samples (Fig. S1 and Table S2). In *A. marina* this phase was superimposed to the non-decaying fluorescence mentioned above.

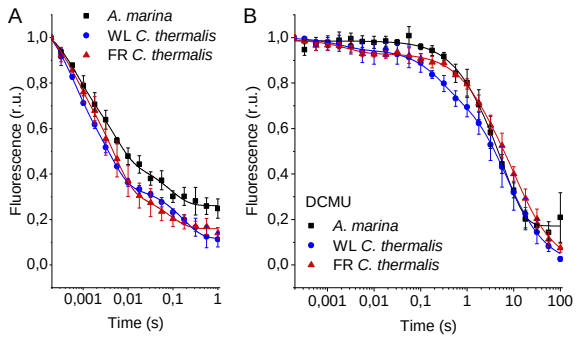

Fig. 2. Fluorescence decay kinetics after a saturating flash in membranes of *A. marina*, WL *C. thermalis* and FR *C. thermalis* with no additions (A) and in presence of DCMU (B). The datapoints represent the averages of three biological replicates, ± s.d., the lines represent the fits of the experimental data. All traces are normalized on the initial variable fluorescence (F_m-F_0). The full 100 s traces of the data in (A) are shown in Fig. S1.

The fluorescence decay due to $S_2Q_A^-$ recombination was measured in presence of the Q_B-site inhibitor, DCMU (Fig. 2B). Decay kinetics associated with $S_2Q_A^-$ recombination were bi-phasic in all samples, but the WL and FR *C. thermalis* also had a fast phase of small amplitude (5-6%) attributed to forward electron transfer in centers in which DCMU was not bound (23). Again, the *A. marina* traces included

a non-decaying phase of fluorescence attributed to centers lacking an intact Mn-cluster. The predominant $S_2Q_A^-$ recombination phase (slow phase in Table S1, amplitude ~80%) was slowest in FR *C. thermalis* (T3 = 10.4±0.8 s), like the slow phase in the absence of DCMU (Table S2).

The fluorescence decay kinetics in membranes of *Synechocystis* sp. PCC6803 (*Synechocystis*), perhaps the best studied Chl-a containing cyanobacterium, were also measured as an additional control. The kinetics in *Synechocystis* membranes were comparable to those reported in Fig. 2 from WL *C. thermalis* (Fig. S2). The *Synechocystis* and *A. marina* fluorescence decay kinetics measured in membranes here are overall slower than those measured in cells previously (24), this difference is ascribed to pH and membrane potential effects further discussed in the Supplementary Information.

To conclude, the forward electron transfer rates from Q_A^- to Q_B/Q_B^- are not significantly different in the three types of PSII. In contrast, the $S_2Q_A^-$ recombination is slower in Chl-f-PSII of FR *C. thermalis* compared to Chl-a-PSII of WL *C. thermalis* and Chl-d-PSII of *A. marina*.

2.2 - S-state turnover efficiency in the far-red PSII

The efficiency of PSII activity can be estimated by the flash-dependent progression through the S-states. This can be measured by thermoluminescence (TL), which arises from radiative recombination of the $S_2Q_B^-$ and $S_3Q_B^-$ states (25). The TL measured in *A. marina*, WL *C. thermalis* and FR *C. thermalis* membranes showed similar flash-dependencies in all three types of PSII (Fig. S3), confirming and extending the earlier report (6). Because the TL data presented some variability between biological replicates (Fig. S3 and associated text), additional analyses were performed by polarography and absorption spectroscopy.

Fig. 3 shows the flash-dependent oxygen evolution measured in *A. marina*, FR *C. thermalis* and *Synechocystis* membranes. The latter were used as a Chl-a-PSII control because the content of PSII in membranes of WL *C. thermalis* was too low to allow accurate O_2 polarography measurements. As shown in Fig. S2, we did not observe any significant difference in forward electron transfer between the two types of Chl-a-PSII used as controls. The measurements were performed using white, red, and far-red flashes. As expected, in dark-adapted samples, with S_1 as the majority state, the maximal O_2 evolution occurred on the 3rd flash with subsequent maxima at 4 flash intervals. These maxima reflect the occurrence of the $S_3/S_4/S_0$ transition in most centers as two water molecules are oxidized, resulting in the release of O_2. This oscillation pattern was the same in all samples and under all excitation conditions, except in *Synechocystis* membranes illuminated with far-red light, where the slow rise in O_2 evolution arises from the weak excitation of Chl-a-PSII by the short wavelength tail of the 730 nm flash.

The miss factor (Fig. 3D) was ≤20% in all the samples except in the *Synechocystis* sample illuminated with far-red flashes (>80%). For *A. marina*, the misses (13-17%) were very similar to those reported earlier (26). The misses for FR *C. thermalis* and for *Synechocystis* when illuminated with the 613 nm

LED were slightly higher (17-20%). The combination of the absence of exogenous electron acceptors, and the relatively long and possibly not fully saturating flashes could have contributed to increasing the miss factors in these measurements. Nevertheless, the polarography data show no major differences between the different types of PSII.

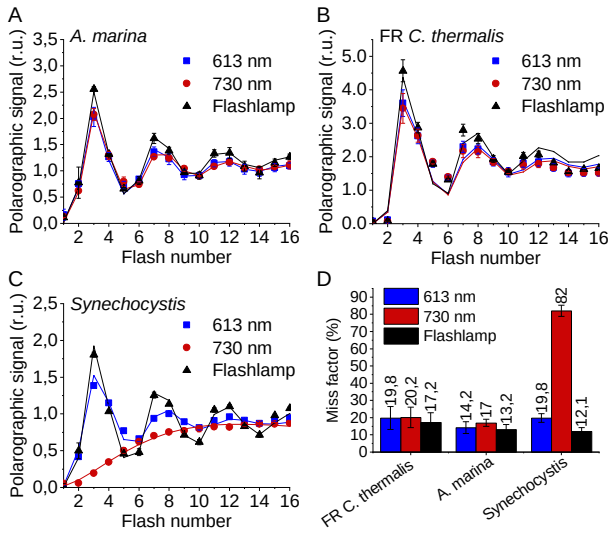

Fig. 3. Flash-induced release of O_2 measured by polarography. (A-C) Patterns of oxygen release in *A. marina*, FR *C. thermalis* and *Synechocystis* membranes. Flashes were given at 900 ms intervals and the O_2 produced after each flash was measured. Flashes were provided by a white xenon flash lamp, a red LED centered at 613 nm, and a far-red LED centered at 730 nm. The data represent the averages of 3 biological replicates ±s.d. The lines represent the fits of the experimental data. (D) Miss factors (in %) calculated from the data shown in (A-C).

Fig. 4 shows the S-state turnover measured as the flash-induced absorption changes at 291 nm, that reflect the redox state of the Mn ions in the oxygen evolving complex (27). These measurements were done in the presence of the electron acceptor, PPBQ, and using single-turnover monochromatic saturating laser flashes. For FR *C. thermalis*, we used partially purified O_2 evolving Chl-f-PSII, while for *A. marina* we used membranes because of difficulties encountered in isolating O_2 evolving PSII. Difficulties were also encountered in isolating O_2 evolving PSII from WL *C. thermalis*, but in this case membranes could not be used because of their high light-scattering properties. Therefore, PSII cores from *T. elongatus* with the D1 isoform PsbA3, which has the highest sequence identity with the D1 of Chl-f-PSII in FR *C. thermalis*, were used as a Chl-a-PSII control (28).

We illuminated the Chl-f-PSII with flashes at wavelengths corresponding to the absorption of the Chl-a bulk (680 nm) and the absorption of long-wavelength chlorophylls (720 to 750 nm) (Fig. 4A). As expected, maximum $\Delta I/I$ occurred on S_2 (flash 1,5,9 etc.) and minimum $\Delta I/I$ on S_0 (flash 3,7,11 etc.). No significant differences could be observed in either the amplitude or the damping of the oscillations between the excitation wavelengths. When using sub-saturating flashes (~83% power), the damping of

the oscillations was the same for all excitation wavelengths (Fig. 4B), verifying that the illumination in Fig. 4A was saturating at all the wavelengths. The equal amplitude of the oscillations obtained at all excitation wavelengths also indicates that the FR *C. thermalis* sample used does not contain any detectable Chl-a-PSII as a contamination. No differences in the oscillation patterns measured in FR *C. thermalis* PSII cores and in *A. marina* membranes were observed (Fig. 4C). The PSII of *T. elongatus* showed a normal S-states progression when using 680 nm excitation, but no oscillation pattern when far-red flashes were used (Fig. 4D).

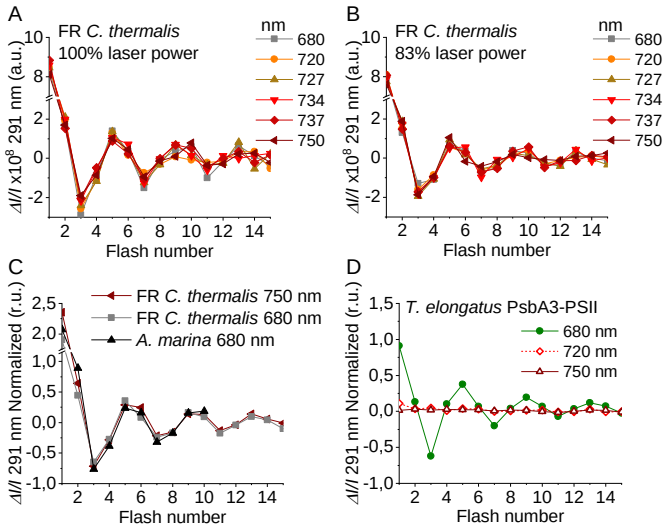

Fig. 4. Flash-induced S-state turnover in FR *C. thermalis* PSII cores, *A. marina* membranes, and *T. elongatus* PsbA3-PSII cores. Absorption changes were measured at 291 nm at 100 ms after each of a series of single-turnover saturating flashes fired with a 300 ms time interval. (A) and (B) Measurements in FR *C. thermalis* PSII cores using flashes at the indicated wavelengths with 100% and 83% laser power (the power of the laser at the different wavelengths is reported in the Supplementary Materials and Methods). (C) Comparison between the absorption changes obtained in FR *C. thermalis* PSII cores and *A. marina* membranes using flashes at the indicated wavelengths (100% laser power). The traces in (C) were normalized on the maximal oscillation amplitude (3rd minus 5th flash). The breaks in the vertical axes in panels (A-C) allow the oscillation pattern to be re-scaled for clarity, because the absorption change on the first flash contains a large non-oscillating component (27) that was not included in the fits. (D) Measurements in isolated *T. elongatus* PsbA3-PSII cores using flashes at the indicated wavelengths.

For all samples the calculated miss factor was ~10% (Fig. S4). The lower miss factor obtained with UV transient absorption compared to polarography is due to the use of laser flashes and of an efficient electron acceptor system.

2.3 - Back-reactions measured by (thermo)luminescence

Charge recombination was investigated by monitoring thermoluminescence and luminescence. The TL curves in Fig. 5A and B show that both Chl-f-PSII and Chl-d-PSII are significantly more luminescent

than Chl-a-PSII, with Chl-f-PSII being the most luminescent. This fits qualitatively with earlier reports (6, 29), despite the variability between biological replicates (Fig. S5 and Table S3). The high luminescence indicates that in the Chl-d-PSII and Chl-f-PSII there is an increase in radiative recombination, although the causes of this increase are likely to be different between the two photosystems, as detailed in the Discussion.

Despite the large difference in TL intensity between the Chl-a-PSII and Chl-f-PSII, their TL peak temperatures were very similar for both $S_2Q_B^-$ and $S_2Q_A^-$ recombination. In Chl-d-PSII, the temperature of the $S_2Q_B^-$ peak was also similar, while the $S_2Q_A^-$ peak was ~15°C lower (Fig. S5 and Table S3). Earlier reports of TL comparing Chl-d-PSII in *A marina* cells with Chl-a-PSII in *Synechocystis* cells also showed that, while the peak position of $S_2Q_B^-$ recombination was similar in the two samples, the $S_2Q_A^-$ peak position was lower in *A. marina* (29), in agreement with the present results in membranes. The peak temperatures measured in cells were lower than the ones reported here, which can be explained by the effect of the transmembrane electric field, as for fluorescence decay, and by the higher heating rate used here (1°C s^{-1} versus 0.33°C s^{-1} used in (29)). When performing the same measurements in *Synechocystis* membranes (Fig. S6), we observed $S_2Q_B^-$ and $S_2Q_A^-$ peak positions comparable to those obtained in the two *C. thermalis* samples.

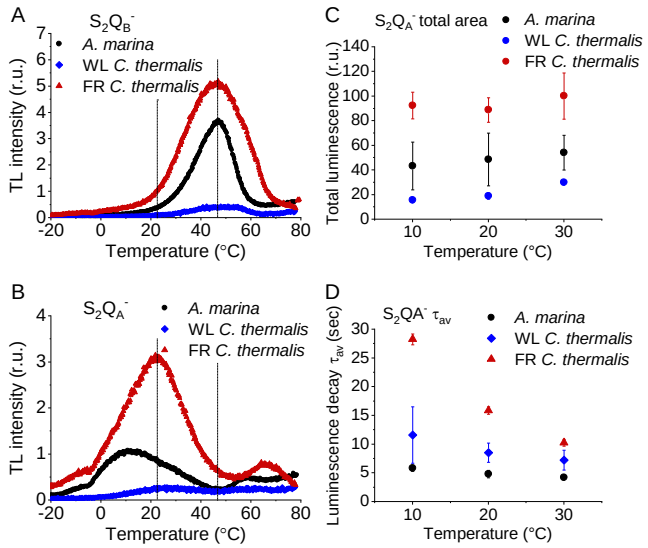

Fig. 5. Thermoluminescence and luminescence measured in *A marina*, WL *C. thermalis* and FR *C. thermalis* membranes. (A) and (B) TL measured in the absence of inhibitors ($S_2Q_B^-$) or in the presence of DCMU ($S_2Q_A^-$), respectively. The signal intensities are normalized on the maximal oxygen evolution rates of each sample. The dashed vertical lines indicate the two peak positions of the FR *C. thermalis* sample. (C) Plots of the total $S_2Q_A^-$ luminescence emission (integrated area below the curves), normalized on the maximal oxygen evolution rate of each sample, at 10, 20 and 30°C. (D) Plots of the average $S_2Q_A^-$ luminescence decay lifetimes (τ_{av}), calculated from the decay phases attributed to $S_2Q_A^-$ recombination, as a function of temperature. In (C) and (D) each point represents the average of 3 biological replicates ±s.d.

The $S_2Q_A^-$ recombination in the presence of DCMU was measured by luminescence decay kinetics at 10, 20 and 30°C, a range of temperatures that covers those of the $S_2Q_A^-$ TL peaks of the three samples. Luminescence decay kinetics were recorded from 570 ms after the flash for 300 seconds. In this time-range, the luminescence arises mainly from recombination via the back-reaction of $S_2Q_A^-$ (30). The total $S_2Q_A^-$ luminescence emission (Fig. 5C) reflected the intensities of the TL peaks, as expected (31), with the order of intensity as follows: Chl-f-PSII > Chl-d-PSII > Chl-a-PSII. The total emissions did not vary significantly between 10 and 30°C, although the decay kinetics were temperature-sensitive (Fig. S7). The decay components identified by fitting the curves and their significance are discussed further in the SI. The luminescence decay attributed to $S_2Q_A^-$ recombination was bi-phasic (Table S4), with the kinetics of both phases being faster in Chl-d-PSII (~3 and ~11 s) than in Chl-a-PSII (~4 and ~25 s), but slower in Chl-f-PSII (~9 and ~39 s). The average $S_2Q_A^-$ luminescence decay lifetimes accelerated with increasing temperature in Chl-a-PSII and Chl-f-PSII but were always faster in Chl-d-PSII (Fig. 5D). The luminescence decay kinetics of the Chl-a-PSII in *Synechocystis* membranes were similar to those measured in WL *C. thermalis* (Fig. S8), suggesting, like the TL data, that the differences in kinetics observed in the two types of far-red PSII are not due to species differences.

Both Chl-f-PSII and Chl-d-PSII show strongly enhanced luminescence, as previously reported (6, 32). However, the Chl-d-PSII differs from the Chl-a-PSII and Chl-f-PSII by having a lower $S_2Q_A^-$ TL peak temperature and a faster $S_2Q_A^-$ luminescence decay. This indicates that Chl-d-PSII has a smaller energy gap between Q_A^- and Phe compared to Chl-a-PSII. In contrast, this energy gap does not appear to be greatly affected or could even be larger in Chl-f-PSII, as suggested by the slower $S_2Q_A^-$ recombination measured by fluorescence (Fig. 2) and luminescence (Fig. 3) decay. The Q_B potentials appear to be largely unchanged, as manifest by the similar $S_2Q_B^-$ stability in all three types of PSII.

2.4 - Singlet oxygen production and sensitivity to high light in the far-red PSII

Fig. 6A shows $^1O_2$ generated by saturating illumination in isolated membranes using histidine as a chemical trap (representative traces in Fig. S10A-C). $^1O_2$ reacts with histidine to form the final oxygenated product, $HisO_2$, resulting in the consumption of O_2, as measured using the O_2 electrode. Without the histidine trap, most $^1O_2$ is thought to be quenched by carotenoids (33). When histidine was present in addition to DCMU, the Chl-d-PSII showed significant light-induced $^1O_2$ formation. Under the same conditions, little $^1O_2$ formation occurred in Chl-a-PSII or Chl-f-PSII in *C. thermalis* membranes. Similarly low levels of $^1O_2$ were generated by Chl-a-PSII in *Synechocystis* membranes (Fig. S10D). Sodium azide, a $^1O_2$ quencher, suppressed the His-dependent oxygen consumption measured in the presence of DCMU, confirming that it was due to the production of $^1O_2$ (Fig. S10E).

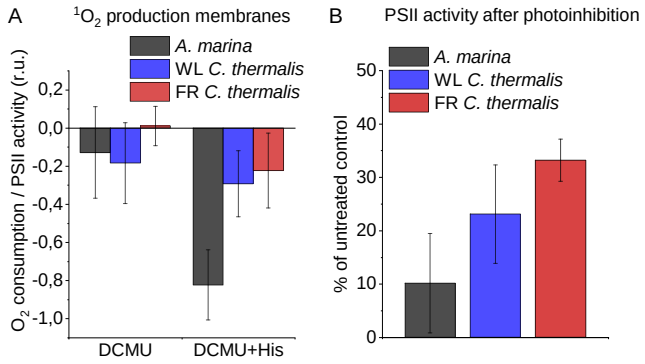

Fig. 6. $^1O_2$ production and PSII sensitivity to high light in *A. marina,* WL *C. thermalis* and FR *C. thermalis* membranes. All samples were used at a chlorophyll concentration of 5 µg ml^{-1}. (A) $^1O_2$ production in presence of DCMU measured as the rate of histidine-dependent consumption of O_2 induced by saturating illumination (xenon lamp, 7100 µmol photons m^{-2} s^{-1}, saturation curves in Fig. S9B and C). The data are averages (±s.d.) of 6 biological replicates for *A. marina* and FR *C. thermalis* and 3 replicates for WL *C. thermalis*. For each replicate, the rates of oxygen consumption were normalized to the maximal oxygen evolution rates measured in presence of DCBQ and ferricyanide. (B) Maximal PSII activities, measured as in (A), after 30 min illumination with saturating red light (660 nm LED, 2600 µmol photons m^{-2} s^{-1}) relative to the maximal activities measured in control samples kept in darkness. The light used for the 30 minutes treatment was as saturating as the xenon lamp used in (A) (Fig. S9D and E). The data are averages of 3 biological replicates ±s.d.

The strikingly high amount of $^1O_2$ generated by Chl-d-PSII prompted us to perform additional controls. i) To test if the high $^1O_2$ was related to the intactness of the PSII donor side, Mn was removed from *A. marina* membranes by Tris-washing. This had little effect on the $^1O_2$ formation with respect to the Mn-containing membranes (Fig. S11), suggesting that the high $^1O_2$ production in untreated *A. marina* membranes does not arise specifically from the fraction of centers that could be devoid of an intact Mn-cluster, responsible for the non-decaying fluorescence observed in Fig. 2B and S1. ii) The possibility that photosystem I (PSI) contributed to the light-induced O_2 consumption by reducing oxygen to $O_2^{\bullet-}$ in membranes was tested (Fig. S12). In the presence of DCMU, PSI-driven O_2 reduction mediated by methyl viologen only took place when exogenous electron donors to PSI were provided. This indicates that there is no contribution from PSI-induced O_2 reduction in Fig. 4A, where exogenous PSI donors are absent. iii) The higher $^1O_2$ production is also seen in *A. marina* cells (Fig. S13A) compared to FR *C. thermalis* cells, and thus is not an artefact associated with the isolation of membranes. WL *C. thermalis* cells also showed low levels of $^1O_2$ production, similar to those measured in membranes (Fig. S13B).

Figure 4B shows the effect of 30 minutes of saturating illumination (red light) on the activity of the Chl-d-PSII, Chl-a-PSII and Chl-f-PSII. The results show that Chl-d-PSII is clearly more susceptible to light induced loss of activity compared to Chl-a-PSII and Chl-f-PSII, because of the high levels of $^1O_2$ production.

3 - Discussion

Here we investigated several functional properties of the two different types of far-red PSII, i) the constitutive Chl-d-PSII of *A. marina*, and ii) the facultative Chl-f-PSII of *C. thermalis*. We compared these properties with each other and with those of standard Chl-a-PSII, looking for differences potentially related to the diminished energy available in the two long-wavelength PSII variants.

3.1 – Forward electron transfer and enzymatic activity

The overall efficiency of electron transfer from water to the PQ pool is comparable in all three types of PSII (independently of the Chl-a-PSII control used), as shown by the near-identical flash patterns of thermoluminescence (Fig. S3) and O_2 release (Fig. 3), both measured without external electron acceptors. When the S-state turnover was measured by following the absorption of the Mn cluster in the UV (Fig. 4), the use of artificial electron acceptors and single-turnover saturating flashes allowed us to obtain better resolved flash patterns that were essentially indistinguishable in all three types of PSII.

In PSII, the damping of the flash patterns of O_2 evolution and of S-state formation is mainly determined by the photochemical "miss factor". These misses, which are typically ~10%, are mainly ascribed to the µs to ms recombination of $S_2TyrZ^{\bullet}Q_A^-$ and $S_3TyrZ^{\bullet}Q_A^-$ states (34). Despite the diminished energy available, the miss factors in both types of the far-red PSII were virtually unchanged compared to Chl-a-PSII, which also suggests that they have the same origin. If so, the energy gaps between TyrZ and P, and thus their redox potentials, would be essentially unchanged. These conclusions agree with those in earlier work on Chl-d-PSII (35) and on Chl-f-PSII (6).

The similar flash-patterns also indicate that, after the primary charge separation, the electron transfer steps leading to water oxidation must have very similar efficiencies in all three types of PSII, i.e. close to 90%, and that major changes in the kinetics of forward electron transfer are unlikely to be present, as pointed out earlier based on less complete data (6). Indeed, electron transfer from Q_A^- to Q_B/Q_B^-, monitored by fluorescence, showed only minor differences in kinetics in the three types of PSII studied (Fig. 2A). The Q_A^- oxidation phase attributed to a PQ binding step was slightly slower in Chl-d-PSII and Chl-f-PSII, possibly reflecting differences in the redox state of the PQ pool between the membrane samples.

3.2 – Back reactions and singlet oxygen production

The most striking difference between the three types of PSII is that the Chl-d-PSII of *A. marina* showed a decreased stability of $S_2Q_A^-$, indicated by the lower temperature of its TL peak and the correspondingly faster luminescent decay kinetics (Fig. 5), and consequently a significant increase in $^1O_2$ generation under high light (Fig. 6A). This likely corresponds to the decrease in the energy gap between Phe and Q_A predicted to result from the ~100 meV lower energy available when using light at ~720 nm to do

photochemistry (6, 15). This is also supported by the estimates in the literature of the redox potential (Em) values of Phe/Phe$^-$ and Q_A/Q_A^- in Mn-containing Chl-d-PSII: compared to Chl-a-PSII, the estimated increase of ~125 meV in the Em of Phe/Phe$^-$ is accompanied by an estimated increase of only ~60 meV in the Em of Q_A/Q_A^-, which implies that a normal energy gap between the excited state of the primary donor (P^*) and P^+Phe^- is maintained but a significant decrease in the energy gap between Phe and Q_A (~325 meV vs ~ 385 meV) is present (36). The changes in the D1 and D2 proteins of *A. marina* responsible for the changes in the Em of Phe/Phe$^-$ and Q_A/Q_A^- are currently unknown. Our results indicate that in Chl-d-PSII, the decrease in the energy gap between Phe and Q_A favors charge recombination by the back-reaction route (via P^+Phe^-), forming the reaction center chlorophyll triplet state (37), which acts as an efficient sensitizer for $^1O_2$ formation (38–41). As a consequence, the Chl-d-PSII is more sensitive to high light than standard Chl-a-PSII (Fig. 6B). The increase in the proportion of recombination going via P^+Phe^- can also result in a higher repopulation of the excited state of the primary donor (P^*), with a consequent increase in radiative decay (high luminescence).

In contrast to the Chl-d-PSII, the Chl-f-PSII shows no increased production of $^1O_2$ and no increased sensitivity to high light compared to Chl-a-PSII, in the conditions tested here (Fig. 6). The back-reactions appear to be little different from the Chl-a-PSII except for the more stable (more slowly recombining) $S_2Q_A^-$, as seen by fluorescence (Fig. 2) and luminescence (Fig. 5) decay. These properties may seem unexpected because this type of PSII has the same energy available for photochemistry as the Chl-d-PSII. In the Chl-d-PSII the lower energy of P^* is matched by an increase in the Em of Phe/Phe$^-$. In the Chl-f-PSII of *C. thermalis* and of the other Chl-f containing species, the Em of Phe/Phe$^-$ is also expected to be increased by the presence, in the far-red D1 isoform, of the strong H-bond from Glu130 (Fig. S14), which is characteristic of high-light D1 variants in cyanobacteria (42). In Chl-a-PSII this change has been reported to induce an increase in the Em of Phe/Phe$^-$ between ~15 and ~30 meV (42, 43): an increase of this size would only fractionally compensate for the ~100 meV decrease in the energy of P^* in Chl-f-PSII, and this would result in a smaller energy gap between P^* and P^+Phe^-. This would favor the repopulation of P^* by back-reaction from P^+Phe^- (even if the repopulation of P^+Phe^- from the $P^+Q_A^-$ state did not increased) and therefore lead to the increased luminescence of Chl-f-PSII, as proposed earlier (6).

The longer lifetime of $S_2Q_A^-$ recombination in Chl-f-PSII indicates that the Em of Q_A/Q_A^- has increased to compensate the up-shift in the Em of Phe/Phe$^-$ and to maintain an energy gap between Phe and Q_A big enough to prevent an increase in reaction center chlorophyll triplet formation. This situation occurs in the PsbA3-D1 high light variant of *T. elongatus*, although the protein changes responsible for the increase in the Em of Q_A/Q_A^- are not known (42). A slower $S_2Q_A^-$ recombination could also arise from an increase in the redox potential of P/P^+ (44, 45), but this would likely compromise forward electron transfer in Chl-f-PSII by decreasing the already diminished reducing power of P^*, which is not what we observe (Fig. 2A).

3.5 – Effects of the pigment composition on the energetics of the far-red PSII

In addition to changes in the redox potentials of Phe and Q_A, the size and pigment composition of the antennas of Chl-d-PSII and Chl-f-PSII could also contribute to the functional differences reported in the present work. These differences are summarized in Fig. 7.

For simplicity, in Fig. 7 and in the text until this point, we have used the terms P^* and P^+Phe^- without making an explicit distinction between Chl_{D1} and P_{D1}. P^* always corresponds to the excited state of Chl_{D1}, however P^+Phe^- includes both $Chl_{D1}^+Phe^-$ and $P_{D1}^+Phe^-$. The energies of these two states are equally affected by changes in the redox potential of Phe/Phe^-. In this section, the discussion requires the first and second radical pairs, $Chl_{D1}^+Phe^-$ and $P_{D1}^+Phe^-$, to be distinguished.

In photosystem II, two factors will determine the yield of charge separation: i) the relative population of the excited state of the Chl_{D1} primary donor, P^*, which depends on the dynamics of excitation energy transfer between pigments, and ii) the rate of population of the second radical pair, $P_{D1}^+Phe^-$, that is more stable (less reversible) than the first radical pair, $Chl_{D1}^+Phe^-$. This rate is determined by the rates of the primary charge separation (forming $Chl_{D1}^+Phe^-$) and of its stabilization by secondary electron transfer (forming $P_{D1}^+Phe^-$), and hence by the energetic of these electron transfer steps.

In the Chl-a-PSII core, the 37 chlorins absorb between ~660 and ~690 nm and are therefore almost isoenergetic to the Chl_{D1} primary donor, P, absorbing at 680 nm. Given the small energy differences, there is little driving force for downhill "funneling" of excitation energy to P, making it a "shallow trap". Different models have been proposed to explain the shallowness of the Chl-a-PSII photochemical trap.

In the trap-limited model, the transfer of excitation between pigments is significantly faster than the electron transfer reactions leading to $P_{D1}^+Phe^-$ formation, and a near-complete equilibration of the excitation energy is established over all pigments, including P, with a distribution that is determined by their individual site energies (46–48). This leads to a low population of P^* (see Table S5), that is diminished as a function of the number of quasi-isoenergetic pigments with which it shares the excitation energy.

In the transfer-to-trap limited model, the small driving force for downhill "funneling" of excitation energy to P causes kinetic bottlenecks for excitation energy equilibration between the core antenna complexes CP43 and CP47 and for excitation energy transfer from these antennas to the reaction center (49–52). In this scenario, there is not a full equilibration of the excitation energy over all pigments, but the relatively slow and reversible energy transfer from the core antennas to the reaction center still leads to a relatively low population of P^*.

Irrespectively of the differences in the details of the kinetic limitation to photochemical trapping between the two models, the common requirement for establishing a high quantum yield of charge

separation is a sufficiently large overall energy gap (~160 meV, (53)) between P^* and $P_{D1}^+Phe^-$, i.e. comprising the primary charge separation (Chl_{D1}^* ↔ $Chl_{D1}^+Phe^-$) and secondary electron transfer ($Chl_{D1}^+Phe^-$ ↔ $P_{D1}^+Phe^-$), shown as a single combined step in Fig. 7. An energy gap of this magnitude is required to avoid rapid recombination to the excited state P^*, thereby limiting the probability of its dissipation via non-photochemical relaxation to the ground state in the antenna (51, 54).

For Chl-d-PSII the antenna system is comparable to that in Chl-a-PSII: all 34 Chl-d molecules, including the primary donor Chl_{D1} at ~720 nm, are close in wavelength and thus both systems are expected to have comparable excitation energy residence on the primary donor (Table S5), irrespective of the rate-limitation model assumed. So Chl-a-PSII and Chl-d-PSII should have the same energetic requirements to ensure a sufficiently high yield of charge separation. Given that the energy of P^* is ~100 meV lower in Chl-d-PSII than in Chl-a-PSII, the energy level of the second and more stable radical pair, $P_{D1}^+Phe^-$, in Chl-d-PSII, needs to be decreased by ~100 meV relative to $P_{D1}^+Phe^-$ in Chl-a-PSII. This corresponds to the published E_m of Phe/Phe^- (36) and the kinetic data (Fig. 5 and 6), as detailed in the previous section.

In *A. marina* membranes, additional Chl-d containing antenna proteins, which form supercomplexes with PSII cores, have been reported to increase the Chl-d-PSII antenna size by almost 200% (55). This will likely result in an increased sharing of the excited state, leading to a diminished population of P^*, and thus a bigger requirement for an energy drop between P^* and $P_{D1}^+Pheo^-$ to ensure efficient charge separation. At the same time, the bigger near-isoenergetic antenna could at least partially explain its higher luminescence, by increasing the probability of P^* decay via radiative emission with respect to photochemical re-trapping (56). This is similar to what happens in plant PSII, where the yield of photochemical trapping of excitation energy is decreased by 10-15% by the association of the Light Harvesting Complex antennas (57).

The pigment layout of Chl-f-PSII is very different, in energy terms, than that of Chl-a-PSII and Chl-d-PSII. The 30 Chl-a molecules are energetically separated from P, absorbing at 720 nm, by >30 nm (>3k_BT). This means excitation energy resides predominantly on P^* and on the other 4 far-red pigments. If the equilibration of the excitation energy between the 5 far-red pigments were significantly faster than charge separation, this pigment arrangement would result in a higher probability of populating P^* in Chl-f-PSII than occurs in Chl-a-PSII and Chl-d-PSII (table S5). The higher P^* population in Chl-f-PSII could ensure that sufficient yield of charge separation is achieved even when the Em of Phe/Phe^- is increased by much less that the 100 meV needed to compensate for the nominally lower energy in P^*, as indicated by the present work. However, thermal equilibration of the excitation energy over the entire antenna in Chl-f-PSII might not occur due to 3 out of the 4 long-wavelength antenna chlorophylls absorbing at longer wavelength than P. This type of antenna energetics could result in rapid excited state equilibration in each of the three main pigment-protein complexes (CP43, CP47 and reaction

center), due to rapid energy transfer from Chl-a to Chl-f/d (with visible light excitation) followed by somewhat slower transfer from the two far-red antenna pools to P, leading to a transfer-to-trap limited bottleneck. As a result, the kinetics of excitation energy transfer from the red and far-red antenna to the reaction center could be more complex than in Chl-a-PSII and Chl-d-PSII, explaining the spread in charge separation kinetics that has been suggested based on ultrafast absorption data (58) and the slower excitation energy trapping kinetics measured by time-resolved fluorescence (59). Despite the slower charge separation, this could be compensated by increased P^* population due to the smaller long wavelength antenna compared to the Chl-d-PSII with its large quasi-isoenergetic antenna.

Despite the upshift in the redox potential of the Phe, and the potentially favorable pigment layout, Chl-f-PSII still suffers from a partial loss in excitation energy trapping efficiency compared to normal PSII (59). This loss is likely manifested in part by its high luminescence (Figure 5 and (6)). This situation suggests that evolution has prioritized the maintenance of the energy gap between Phe and Q_A, which minimizes harmful charge recombination, over photochemical quantum efficiency.

The increased photosensitivity seen in Chl-d-PSII, which is attributed to the smaller energy gap between Phe and Q_A (~325meV), is avoided in Chl-f-PSII by maintaining a large energy gap between Phe and Q_A (~385meV) (Fig. 7). This inevitably results in a decreased driving force for charge separation due to the smaller energy gap between P^* and $P_{D1}^+Pheo^-$ (Fig. 8), estimated to be ~ 80 meV in Chl-f-PSII compared to ~ 160 meV in Chl-a-PSII and Chl-f-PSII. However, because of the decreased dilution of the excitation energy on P^* arising from the small number of long-wavelength antenna pigments, this results in only a small loss of trapping efficiency (59) and a near-negligible effect on enzyme turnover efficiency (Figures 2-4 and (6)).

This energetic balancing trick in Chl-f-PSII, which allows both high enzyme efficiency and high resilience to photodamage despite working with 100 meV less energy, comes with a very significant disadvantage: its absorption cross-section at long wavelength is ~7 times smaller than that of the standard core Chl-a-antenna. This makes sense as this system has evolved as a facultative survival mechanism, that is not advantageous when visible light is available.

In contrast, Chl-d-PSII seems to have maximized light collection at long wavelengths (with its full-size far-red antenna) and maximized the yield of charge separation (by maintaining the full P^* to P^+Phe^- driving force). However, the energy shortfall at long wavelength is lost from the "energy headroom" (mainly from the transmembrane energy gap between Phe and Q_A) that is proposed to minimize harmful charge recombination by buffering the effects of pulses of the trans-membrane electric field associated with fluctuations in light intensity (16, 60). This seems to correspond well to the shaded and stable epiphytic niche that *A. marina* occupies (7, 61–64).

Chl-d-PSII and Chl-f-PSII have evolved different strategies to do oxygenic photosynthesis in far-red light and have been impacted differently by the decrease in energy available. Understanding how the

redox tuning of the electron transfer cofactors and the layout of the far-red pigments determine the trade-off between efficiency and resilience in PSII is a necessary step to inform strategies aimed at using far-red photosynthesis for agricultural and biotechnological applications. Photosynthesis, it seems, can break the red limit but not the "law" that states there is no such thing as a free lunch.

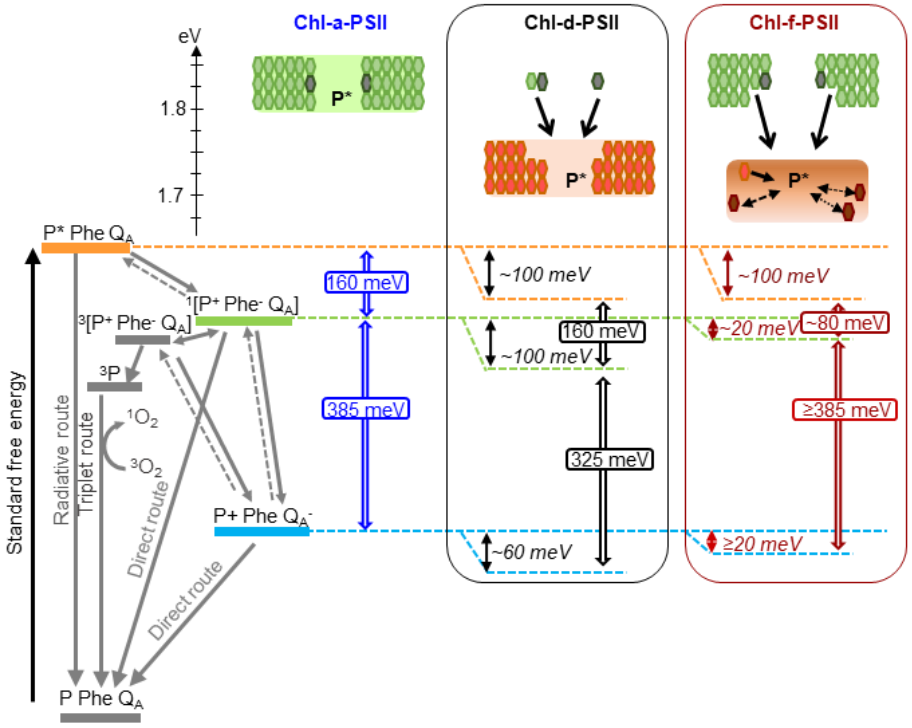

Fig. 7. Model of the energy differences in Chl-a-PSII, Chl-d-PSII and Chl-f-PSII. The top part of the figure represents the localization of the excitation energy over the antenna pigments and P* (energies in eV, scale on the left side). The localization of the excitation energy is indicated by the colored boxes (green for Chl-a, orange for Chl-d and brown for Chl-f), without necessarily assuming a full equilibration (see main text). In Chl-a-PSII, the excitation is distributed over P, 34 antenna Chl-a (light green) and 2 Phe-a (dark grey); in Chl-d-PSII, the excitation is distributed over P and 31 antenna Chl-d (orange) but not over the 1 Chl-a and 2 Phe-a, that transfer excitation downhill to the Chl-d pigments (black arrows); in Chl-f-PSII, the excitation is distributed only over P, one Chl-d and 3 Chl-f (brown), while the remaining 29 Chl-a and 2 Phe-a transfer excitation energy downhill to the far-red pigments. In Chl-f-PSII, 3 of the far-red antenna pigments are at longer wavelength than P, so transfer of excitation energy from them to P is less efficient (dashed and dotted black arrows). The grading of the colored box for Chl-f represents uncertainty in the degree of excited state sharing between the longest wavelength chlorophylls and P. The bottom part of the figure represents, on the left, the energetics of the radical pairs and the recombination routes in PSII. The horizontal dashed lines represent the standard free energies of P^* (orange), P^+Phe^- (light green) and $P^+Q_A^-$ (light blue). Note that the electron transfer between P^* and P^+Phe^- includes two steps, the primary charge separation leading to $Chl_{D1}{}^+Phe^-$ formation and the secondary stabilization leading to $P_{D1}{}^+Phe^-$ formation, but here represented as a single step for simplicity. The free energy gaps between P^* and P^+Phe^- and between

P^+Phe^- and $P^+Q_A^-$ in Chl-a-PSII (blue) and our current estimates for Chl-d-PSII (black) and Chl-f-PSII (dark red) are represented on the right.

4 – Materials and Methods

4.1 – Cyanobacterial growth

Acaryochloris marina was grown in a modified liquid K-ESM medium containing 14 µM iron (65), at 30°C under constant illumination with far-red light (750 nm, Epitex; L750-01AU) at ~30 µmol photons m^{-2} s^{-1}. *Chroococcidiopsis thermalis* PCC7203 was grown in liquid BG11 medium (66) at 30°C, under two illumination conditions: white light at ~30 µmol photons m^{-2} s^{-1} (for WL *C. thermalis* samples) and far-red light (750 nm, Epitex; L750-01AU) at ~30 µmol photons m^{-2} s^{-1} (for FR *C. thermalis* samples). *Synechocystis sp.* PCC 6803 was grown in liquid BG11 medium at 30°C under constant illumination with white light at ~30 µmol photons m^{-2} s^{-1}. The *Thermosynechococcus elongatus ΔpsbA1, ΔpsbA2* deletion mutant (28) was grown in liquid DNT medium at 45°C.

4.2 – Isolation of membranes and PSII cores

Membranes were prepared as described in the Supplementary Materials and Methods, frozen in liquid nitrogen and stored at -80°C until use. Partially purified *C. thermalis* PSII cores retaining oxygen evolution activity were isolated by anion exchange chromatography using a 40 ml DEAE column. The column was equilibrated with 20 mM MES-NaOH pH 6.5, 5 mM $CaCl_2$, 5 mM $MgCl_2$ and 0.03% (w/v) β-DM (n-Dodecyl-β-D-maltoside) and elution was done using a linear gradient of $MgSO_4$ from 0 to 200 mM in 100 min, with a flow rate of 4 ml min^{-1}. Fractions enriched in PSII were pooled, frozen in liquid nitrogen and stored at -80°C. PSII-PsbA3 cores from *T. elongatus* WT*3 were purified as previously described (53).

4.3 – Fluorescence

Flash-induced chlorophyll fluorescence and its subsequent decay were measured with a fast double modulation fluorimeter (FL 3000, PSI, Czech Republic). Excitation was provided by a single saturating 70 µs flash at 630 nm and the decay in Q_A^- concentration was probed in the 100 µs to 100 s time region using non-actinic measuring pulses following a logarithmic profile as described in (19). Details on the analysis of the fluorescence curves are provided in the Supplementary Materials and Methods. Membrane samples were adjusted to a total chlorophyll concentration of 5 µg Chl ml^{-1} in resuspension buffer, pre-illuminated with room light for 10 seconds and then kept in the dark on ice until used for measurements. Measurements were performed at 20°C. Where indicated, 20 µM DCMU (3-(3,4-dichlorophenyl)-1,1-dimethylurea) was used.

4.4 – Thermoluminescence and luminescence

Thermoluminescence curves and luminescence decay kinetics were measured with a lab-built apparatus, described in (67). Membrane samples were diluted in resuspension buffer to a final concentration of 5 µg Chl ml^{-1} in the case of *A. marina* and FR *C. thermalis* and of 10 µg ml^{-1} in the case of WL *C. thermalis* and *Synechocystis*. The samples were pre-illuminated with room light for 10 seconds and then kept in the dark on ice for at least one hour before the measurements. When used, 20 µM DCMU was added to the samples before the pre-illumination step. Excitation was provided by single turnover saturating laser flashes (Continuum Minilite II, frequency doubled to 532 nm, 5 ns FWHM). Details on the measurement conditions and on the analysis of the luminescence decay kinetics are provided in the Supplementary Materials and Methods.

4.5 – Oxygen evolution and consumption rates

Oxygen evolution and consumption rates were measured with a Clark-type electrode (Oxygraph, Hansatech) at 25°C. Membrane samples were adjusted to a total chlorophyll concentration of 5 µg Chl ml^{-1}. Illumination was provided by a white xenon lamp filtered with a heat filter plus red filter, emitting 600-700 nm light at 7100 µmol photons m^{-2} s^{-1} (Quantitherm light meter, Hansatech). When required, the light intensity was reduced by using neutral density filters (Thorlabs). For PSII maximal oxygen evolution rates, 1 mM DCBQ (2,5-Dichloro-1,4-benzoquinone) and 2 mM potassium ferricyanide were used as an electron acceptor system. Photoinhibitory illumination was performed at room temperature for 30 min with a lab-built red LED (660 nm, 2600 µmol photons m^{-2} s^{-1}). For histidine-mediated chemical trapping of singlet oxygen, 20 µM DCMU, 5 mM L-Histidine and, where specified, 10 mM sodium azide (NaN_3) were used. PSI activity was measured as the rate of oxygen consumption in presence of 20 µM DCMU and 100 µM methyl viologen using 5 mM sodium ascorbate and 50 µM TMPD (N,N,N′,N′-tetramethyl-p-phenylenediamine) as electron donors.

4.6 – Flash-dependent oxygen evolution with Joliot electrode

Time-resolved oxygen polarography was performed using a custom-made centrifugable static ring-disk electrode assembly of a bare platinum working electrode and silver-ring counter electrode, as previously described (68). For each measurement, membranes equivalent to 10 µg of total chlorophyll were used. Three different light sources were used to induce the S-state transitions: a red LED (613 nm), a far-red LED (730 nm) and a Xenon flashlamp. Details on the experimental setup and on the lights used are provided in the Supplementary Materials and Methods. Measurements were performed at 20°C. For each measurement, a train of 40 flashes fired at 900 ms time interval was given and the flash-induced oxygen-evolution patterns were taken from the maximal O_2 signal of each flash and fitted with an extended Kok model as described in (26).

4.7 – UV transient absorption

UV pump-probe absorption measurements were performed using a lab-built Optical Parametric Oscillator (OPO)-based spectrophotometer (69) with a time resolution of 10 ns and a spectral resolution of 2 nm (see Supplementary Materials and Methods for details on the setup). Samples were diluted in resuspension buffer to a final concentration of 25 µg Chl ml^{-1} for isolated *C. thermalis* and *T. elongatus* PSII cores and 40 µg Chl ml^{-1} for *A. marina* membranes. Samples were pre-illuminated with room light for 10 seconds and then kept in the dark on ice for at least one hour before the measurements. 100 µM PPBQ (Phenyl-p-benzoquinone) was added just before the measurements. The sample was refreshed between each train of flashes. For each measurement, a train of 20 flashes (6 ns FWHM) fired at 300 ms time interval was given, and absorption changes measured at 100 ms after each flash.

Acknowledgements

This work was supported by BBSRC grants BB/R001383/1, BB/V002015/1 and BB/R00921X. Julien Sellés acknowledges funding from the Labex Dynamo (ANR-11-LABX-0011-01). AB has been in part supported by the French Infrastructure for Integrated Structural Biology (FRISBI) ANR-10-INBS-05.

Competing interests: The authors declare no competing interests. Data and materials availability: All data are available in the manuscript or the supplementary material.

Authors contributions

A.W.R., S.V. and A.F. conceived the study; S.V. performed the fluorescence, (thermo)luminescence, luminescence and oxygen evolution measurements and analyzed the data together with A.F. and A.W.R.; W.R. performed the photoinhibition measurements and analyzed the data; D.N. and R.A. performed the polarography measurements and analyzed the data with the help of H.D.; J.S., A.B. and S.V. performed the UV transient absorption measurements and analyzed the data; S.S. contributed to data analysis and interpretation; S.V. and A.W.R. wrote the manuscript, with contributions from A.B., R.A., S.S., H.D. and A.F.. All authors approved the manuscript.

References

1. Diner BA, Rappaport F (2002) Structure, dynamics, and energetics of the primary photochemistry of Photosystem II of oxygenic photosynthesis. *Annu Rev Plant Biol* 53:551–580.

2. Holzwarth AR, et al. (2006) Kinetics and mechanism of electron transfer in intact photosystem

II and in the isolated reaction center: Pheophytin is the primary electron acceptor. *Proc Natl Acad Sci U S A* 103(18):6895–6900.

3. Romero E, Van Stokkum IHM, Novoderezhkin VI, Dekker JP, Van Grondelle R (2010) Two different charge separation pathways in photosystem II. *Biochemistry* 49(20):4300–4307.

4. Cardona T, Sedoud A, Cox N, Rutherford AW (2012) Charge separation in Photosystem II: A comparative and evolutionary overview. *Biochim Biophys Acta - Bioenerg* 1817(1):26–43.

5. Rutherford AW, Osyczka A, Rappaport F (2012) Back-reactions, short-circuits, leaks and other energy wasteful reactions in biological electron transfer: Redox tuning to survive life in O 2. *FEBS Lett* 586(5):603–616.

6. Nürnberg DJ, et al. (2018) Photochemistry beyond the red limit in chlorophyll f–containing photosystems. *Science (80-)* 360(6394):1210–1213.

7. Miyashita H, et al. (1996) Chlorophyll d as a major pigment. *Nature* 383(6599):402.

8. Renger T, Schlodder E (2008) The primary electron donor of photosystem II of the cyanobacterium acaryochloris marina is a chlorophyll d and the water oxidation is driven by a chlorophyll a/chlorophyll d heterodimer. *J Phys Chem B* 112(25):7351–7354.

9. Schlodder E, et al. (2007) Both chlorophylls a and d are essential for the photochemistry in photosystem II of the cyanobacteria, Acaryochloris marina. *Biochim Biophys Acta - Bioenerg* 1767(6):589–595.

10. Chen M, et al. (2010) A Red-Shifted Chlorophyll. *Science (80-)* 329(5997):1318–1319.

11. Gan F, et al. (2014) Extensive remodeling of a cyanobacterial photosynthetic apparatus in far-red light. *Science (80-)* 345(6202):1312–1317.

12. Judd M, et al. (2020) The primary donor of far-red photosystem II: ChlD1 or PD2? *Biochim Biophys Acta - Bioenerg* 1861(10):148248.

13. Gisriel CJ, et al. (2022) Structure of a monomeric photosystem II core complex from a cyanobacterium acclimated to far-red light reveals the functions of chlorophylls d and f. *J Biol Chem* 298(1):101424.

14. Umena Y, Kawakami K, Shen JR, Kamiya N (2011) Crystal structure of oxygen-evolving photosystem II at a resolution of 1.9Å. *Nature* 473(7345):55–60.

15. Cotton CAR, et al. (2015) Photosynthetic constraints on fuel from microbes. *Front Bioeng Biotechnol* 3(MAR):1–5.

16. Davis GA, et al. (2016) Limitations to photosynthesis by proton motive force-induced photosystem II photodamage. *Elife* 5:1–27.

17. Chen M, Blankenship RE (2011) Expanding the solar spectrum used by photosynthesis. *Trends Plant Sci* 16(8):427–431.

18. Crofts AR, Wraight CA (1983) The electrochemical domain of photosynthesis. *Biochim Biophys Acta - Rev Bioenerg* 726(3):149–185.

19. Vass I, Kirilovsky D, Etienne AL (1999) UV-B radiation-induced donor- and acceptor-side modifications of photosystem II in the cyanobacterium Synechocystis sp. PCC 6803. *Biochemistry* 38(39):12786–12794.

20. De Wijn R, Van Gorkom HJ (2001) Kinetics of electron transfer from QA to QB in photosystem II. *Biochemistry* 40(39):11912–11922.

21. Nixon PJ, Trost JT, Diner BA (1992) Role of the carboxy-terminus of polypeptide D1 in the assembly of a functional water-oxidizing manganese cluster in photosystem II of the

cyanobacterium Synechocystis sp. PCC 6803:assembly requires a free carboxyl group at C-terminal position 344. *Biochemistry* 31(44):10859–10871.

22. Debus RJ, Campbell KA, Pham DP, Hays AMA, Britt RD (2000) Glutamate 189 of the D1 polypeptide modulates the magnetic and redox properties of the manganese cluster and tyrosine Y(Z) in photosystem II. *Biochemistry* 39(21):6275–6287.

23. Lavergne J (1982) Mode of action of 3-(3,4-dichlorophenyl)-1,1-dimethylurea. Evidence that the inhibitor competes with plastoquinone for binding to a common site on the acceptor side of Photosystem II. *Biochim Biophys Acta - Bioenerg* 682(3):345–353.

24. Cser K, Deák Z, Telfer A, Barber J, Vass I (2008) Energetics of Photosystem II charge recombination in Acaryochloris marina studied by thermoluminescence and flash-induced chlorophyll fluorescence measurements. *Photosynth Res* 98(1–3):131–140.

25. Rutherford AW, Crofts AR, Inoue Y (1982) Thermoluminescence as a probe of Photosystem II photochemistry. The origin of the flash-induced glow peaks. *BBA - Bioenerg* 682(3):457–465.

26. Nöring B, Shevela D, Renger G, Messinger J (2008) Effects of methanol on the Si-state transitions in photosynthetic water-splitting. *Photosynth Res* 98(1–3):251–260.

27. Lavergne J (1991) Improved UV-visible spectra of the S-transitions in the photosynthetic oxygen-evolving system. *Biochim Biophys Acta - Bioenerg* 1060(2):175–188.

28. Sugiura M, Boussac A, Noguchi T, Rappaport F (2008) Influence of Histidine-198 of the D1 subunit on the properties of the primary electron donor, P680, of photosystem II in Thermosynechococcus elongatus. *Biochim Biophys Acta - Bioenerg* 1777(4):331–342.

29. Cser K, Deák Z, Telfer A, Barber J, Vass I (2008) Energetics of Photosystem II charge recombination in Acaryochloris marina studied by thermoluminescence and flash-induced chlorophyll fluorescence measurements. *Photosynth Res* 98(1–3):131–140.

30. Goltsev V, Zaharieva I, Chernev P, Strasser RJ (2009) Delayed fluorescence in photosynthesis. *Photosynth Res* 101(2–3):217–232.

31. Rutherford AW, Inoue Y (1984) Oscillation of delayed luminescence from PS II: recombination of S2Q-B and S3Q-B. *FEBS Lett* 165(2):163–170.

32. Cser K, Vass I (2007) Radiative and non-radiative charge recombination pathways in Photosystem II studied by thermoluminescence and chlorophyll fluorescence in the cyanobacterium Synechocystis 6803. *Biochim Biophys Acta - Bioenerg* 1767(3):233–243.

33. Telfer A, Bishop SM, Phillips D, Barber J (1994) Isolated photosynthetic reaction center of photosystem II as a sensitizer for the formation of singlet oxygen. Detection and quantum yield determination using a chemical trapping technique. *J Biol Chem* 269(18):13244–13253.

34. Grabolle M, Dau H (2007) Efficiency and role of loss processes in light-driven water oxidation by PSII. *Physiol Plant* 131(1):50–63.

35. Shevela D, Nöring B, Eckert HJ, Messinger J, Renger G (2006) Characterization of the water oxidizing complex of photosystem II of the Chl d-containing cyanobacterium Acaryochloris marina via its reactivity towards endogenous electron donors and acceptors. *Phys Chem Chem Phys* 8(29):3460–3466.

36. Allakhverdiev SI, et al. (2011) Redox potentials of primary electron acceptor quinone molecule (Q A)- and conserved energetics of photosystem II in cyanobacteria with chlorophyll a and chlorophyll d. *Proc Natl Acad Sci U S A* 108(19):8054–8058.

37. Rutherford AW, Paterson DR, Mullet JE (1981) A light-induced spin-polarized triplet detected by EPR in Photosystem II reaction centers. *BBA - Bioenerg* 635(2):205–214.

38. Johnson GN, Rutherford AW, Krieger A (1995) A change in the midpoint potential of the quinone QA in Photosystem II associated with photoactivation of oxygen evolution. *BBA - Bioenerg* 1229(2):202–207.

39. Keren N, Gong H, Ohad I (1995) Oscillations of reaction center II-D1 protein degradation in vivo induced by repetitive light flashes: Correlation between the level of RCII-Q-B and protein degradation in low light. *J Biol Chem* 270(2):806–814.

40. Keren N, Ohad I, Rutherford AW, Drepper F, Krieger-Liszkay A (2000) Inhibition of Photosystem II activity by saturating single turnover flashes in calcium-depleted and active Photosystem II. *Photosynth Res* 63(3):209–216.

41. Vass I, Cser K (2009) Janus-faced charge recombinations in photosystem II photoinhibition. *Trends Plant Sci* 14(4):200–205.

42. Sugiura M, et al. (2010) Energetics in Photosystem II from Thermosynechococcus elongatus with a D1 protein encoded by either the psbA1 or psbA3 gene. *Biochim Biophys Acta - Bioenerg* 1797(8):1491–1499.

43. Merry SAP, et al. (1998) Modulation of Quantum Yield of Primary Radical Pair Formation in Photosystem II by Site-Directed Mutagenesis Affecting Radical Cations and Anions. *Biochemistry* 37(50):17439–17447.

44. Diner BA, et al. (2001) Site-directed mutations at D1-His198 and D2-His197 of photosystem II in Synechocystis PCC 6803: Sites of primary charge separation and cation and triplet stabilization. *Biochemistry* 40(31):9265–9281.

45. Sugiura M, Ozaki Y, Rappaport F, Boussac A (2016) Corrigendum to “Influence of Histidine-198 of the D1 subunit on the properties of the primary electron donor, P680, of photosystem II in Thermosynechococcus elongatus.” *Biochim Biophys Acta - Bioenerg* 1857(12):1943–1948.

46. Mieghem F van, et al. (1995) Charge Recombination Reactions in Photosystem II. 1. Yields, Recombination Pathways, and Kinetics of the Primary Pair. *Biochemistry* 34(14):4798–4813.

47. Schatz GH, Brock H, Holzwarth AR (1987) Picosecond kinetics of fluorescence and absorbance changes in photosystem II particles excited at low photon density. *Proc Natl Acad Sci* 84(23):8414–8418.

48. Dau H, Sauer K (1996) Exciton equilibration and photosystem II exciton dynamics - A fluorescence study on photosystem II membrane particles of spinach. *Biochim Biophys Acta - Bioenerg* 1273(2):175–190.

49. Jennings RC, Elli G, Garlaschi FM, Santabarbara S, Zucchelli G (2000) Selective quenching of the fluorescence of core chlorophyll-protein complexes by photochemistry indicates that Photosystem II is partly diffusion limited. *Photosynth Res* 66(3):225–233.

50. Pawlowicz NP, Groot ML, Van Stokkum IHM, Breton J, Van Grondelle R (2007) Charge separation and energy transfer in the photosystem II core complex studied by femtosecond midinfrared spectroscopy. *Biophys J* 93(8):2732–2742.

51. Raszewski G, Renger T (2008) Light harvesting in photosystem II core complexes is limited by the transfer to the trap: Can the core complex turn into a photoprotective mode? *J Am Chem Soc* 130(13):4431–4446.

52. Kaucikas M, Maghlaoui K, Barber J, Renger T, Van Thor JJ (2016) Ultrafast infrared observation of exciton equilibration from oriented single crystals of photosystem II. *Nat Commun* 7:1–8.

53. Sugiura M, et al. (2014) Modification of the pheophytin redox potential in Thermosynechococcus elongatus Photosystem II with PsbA3 as D1. *Biochim Biophys Acta -*

Bioenerg 1837(1):139–148.

54. Schatz GH, Brock H, Holzwarth AR (1988) Kinetic and Energetic Model for the Primary Processes in Photosystem II. *Biophys J* 54(3):397–405.

55. Chen M, Bibby TS, Nield J, Larkum AWD, Barber J (2005) Structure of a large photosystem II supercomplex from Acaryochloris marina. *FEBS Lett* 579(5):1306–1310.

56. Rappaport F, Lavergne J (2009) Thermoluminescence: Theory. *Photosynth Res* 101(2–3):205–216.

57. Engelmann ECM, Zucchelli G, Garlaschi FM, Casazza AP, Jennings RC (2005) The effect of outer antenna complexes on the photochemical trapping rate in barley thylakoid Photosystem II. *Biochim Biophys Acta - Bioenerg* 1706(3):276–286.

58. Zamzam N, et al. (2020) Femtosecond visible transient absorption spectroscopy of chlorophyll-f-containing photosystem II. *Proc Natl Acad Sci* 117(37):23158–23164.

59. Mascoli V, Bersanini L, Croce R (2020) Far-red absorption and light-use efficiency trade-offs in chlorophyll f photosynthesis. *Nat Plants* 6(8):1044–1053.

60. Davis GA, Rutherford AW, Kramer DM (2017) Hacking the thylakoid proton motive force for improved photosynthesis: modulating ion flux rates that control proton motive force partitioning into Δ ψ and ΔpH. *Philos Trans R Soc B Biol Sci* 372(1730):20160381.

61. Murakami A, Miyashita H, Iseki M, Adachi K, Mimuro M (2004) Chlorophyll d in an Epiphytic Cyanobacterium of Red Algae. *Science (80-)* 303(5664):1633.

62. Miller SR, et al. (2005) Discovery of a free-living chlorophyll d -producing cyanobacterium with a hybrid proteobacterial/cyanobacterial small-subunit rRNA gene. *Proc Natl Acad Sci* 102(3):850–855.

63. Kühl M, Chen M, Ralph PJ, Schreiber U, Larkum AWD (2005) Ecology: A niche for cyanobacteria containing chlorophyll d. *Nature* 433(7028):820.

64. Mohr R, et al. (2010) A new chlorophyll d-containing cyanobacterium: Evidence for niche adaptation in the genus Acaryochloris. *ISME J* 4(11):1456–1469.

65. Bailleul B, et al. (2008) The thermodynamics and kinetics of electron transfer between cytochrome b6f and photosystem I in the chlorophyll d-dominated cyanobacterium, Acaryochloris marina. *J Biol Chem* 283(37):25218–25226.

66. Rippka R, Deruelles J, Waterbury JB (1979) Generic assignments, strain histories and properties of pure cultures of cyanobacteria. *J Gen Microbiol* 111(1):1–61.

67. De Causmaecker S (2018) Bioenergetic Studies on the Quinone Electron Acceptors of Photosystem II. doi:10.25560/68272.

68. Dilbeck PL, et al. (2012) The D1-D61N mutation in Synechocystis sp. PCC 6803 allows the observation of pH-sensitive intermediates in the formation and release of O 2 from photosystem II. *Biochemistry* 51(6):1079–1091.

69. Joliot P, Béal D, Rappaport F (1998) A New High-Sensitivity 10-ns Time-Resolution Spectrophotometric Technique Adapted to In Vivo Analysis of the Photosynthetic Apparatus. *Photosynthesis: Mechanisms and Effects* (Springer Netherlands, Dordrecht), pp 4247–4252.